Petroleum Science 19 (2022) 2420–2430

Contents lists available at ScienceDirect

Petroleum Science

journal homepage: www.keaipublishing.com/en/journals/petroleum-science

Original Paper

Investigations on methane hydrate formation, dissociation, and viscosity in gas-water-sand system

Shang-Fei Song [a], Shun-Kang Fu [b], Qing-Yun Liao [a], Bo-Hui Shi [a, **], Hong-Ju Chen [a, c], Jing Gong [a, *]

[a] State Key Laboratory of Natural Gas Hydrates/ National Engineering Laboratory for Pipeline Safety, China University of Petroleum, Beijing, 102249, China
[b] PipeChina West East Pipeline Company, Shanghai, 200122, China
[c] Key Lab of Deepwater Engineering, CNOOC Research Institute, Beijing, 100028, China

ARTICLE INFO

Article history:
Received 3 January 2022
Received in revised form
11 July 2022
Accepted 12 July 2022
Available online 16 July 2022

Edited by Xiu-Qiu Peng

Keywords:
Hydrate slurry
Micron-sized sands
Hydrate formation
Hydrate dissociation
Viscosity characteristics

ABSTRACT

Understanding the kinetics and viscosity of hydrate slurry in gas-water-sand system is of great significance for the high-efficiency and high-safety development of natural gas hydrates. The effect of micron-sized sands with various concentrations and particle sizes on the hydrate formation, dissociation, and viscosity in gas-water-sand system are investigated in this work. The experimental results show that the hydrate induction time in the sandy system is slightly prolonged compared to the pure gas-water system, and the inhibition effect first strengthens and then weakens as the sand concentration increases from 0 wt% to 5 wt%. Besides, the difference of hydrate formation amount in various cases is not obvious. The concentration and particle size of sand have little effect on the kinetics of hydrate formation. Both promoting and inhibiting effects on hydrate formation have been found in the sandy multiphase fluid. For the viscosity characteristics, there are three variations of hydrate slurry viscosity during the formation process: Steep drop type, S-type and Fluctuation type. Moreover, appropriate sand size is helpful to reduce the randomness of slurry viscosity change. Meanwhile, even at the same hydrate volume fraction, the slurry viscosity in the formation process is significantly higher than that in dissociation process, which needs further research. This work provides further insights of hydrate formation, dissociation, and viscosity in gas-water-sand system, which is of great significance for safe and economic development of natural gas hydrates.

1. Introduction

Natural Gas Hydrates (NGHs) are non-stoichiometric crystal solids composed of water and small molecular gases, such as methane, ethane, and carbon dioxide etc. Natural gas molecules (mainly CH_4) are physically wrapped in hydrate clathrate cages (Englezos, 1993; Song et al., 2019). NGHs are known as important energy resources in the future, since twice carbon content of fossil fuels is estimated in the global natural gas hydrate resources (Englezos, 2019; Hong et al., 2020; Zhu et al., 2021). Several methods for exploiting and developing NGHs have been applied in pilot test by several countries, including depressurization method, thermal method, CH_4–CO_2 replacement method, solid fluidization method and so on (Shi et al., 2021; Zhou et al., 2017).

Natural gas hydrates are prevalent in ultralow-permeability fine-grained sediments with substantial reserves. However, the efficient and safe production of natural gas from fine-grained hydrate reservoirs remains a global challenge. The micron-sized sand particles in the reservoirs are easily entrapped by the produced water and flows upward in the flowline (Liao et al., 2022; Liu et al., 2021). In addition, hydrates are easy to re-formation in the flowline due to the low seawater temperature.

The efficiency of gas production will be reduced in the presence of sand deposition and hydrate deposition. Under extreme scenarios, the flowline will be blocked and gas production will be forced to stop. Therefore, understanding the kinetics and viscosity of hydrate slurry in gas-water-sand system is of great significance to high-efficiency and high-safety development of natural gas hydrates.

To understand how NGHs form and flow with the presence of

* Corresponding author.
** Corresponding author.
E-mail addresses: bh.shi@cup.edu.cn (B.-H. Shi), ydgj@cup.edu.cn (J. Gong).

https://doi.org/10.1016/j.petsci.2022.07.001

sands is important for avoiding the NGHs re-formation and flowline blocking during the large-scale exploitation and development of NGHs. Most work has been reported about the influences of sand particles on NGHs formation/dissociation in several aspects, such as the heterogeneous nucleation site effect (Ahuja et al., 2018; Govindaraj et al., 2015; Heeschen et al., 2016; Linga et al., 2012; Nesterov et al., 2015; Pan et al., 2018; Prasad et al., 2012; Raman et al., 2016; Shi et al., 2018; Siangsai et al., 2015; Wang et al., 2017; Zi et al., 2019), pore improving formation effect (Jin et al., 2012; Nair et al., 2016; Zhong et al., 2015), particle collision effect (Wang et al., 2017), heat transfer effect (Kang and Lee, 2010; Pan et al., 2018; Wen et al., 2019; Yang et al., 2012; Zhang et al., 2010) and so on.

Several researches indicated that sand particles could serve as hydrate nucleation sites to promote the hydrate formation in water system, and shorten hydrate induction time by reducing the randomness of hydrate nucleation (Ahuja et al., 2018; Govindaraj et al., 2015; Heeschen et al., 2016; Linga et al., 2012; Nesterov et al., 2015; Pan et al., 2018; Prasad et al., 2012; Raman et al., 2016; Shi et al., 2018; Siangsai et al., 2015; Wang et al., 2017; Zi et al., 2019). The addition of sand particles significantly increases the gas-water interface area and helps to disperse the aqueous phase (Chari et al., 2013). This effect is usually found at a lower sand dosage (Wang et al., 2019a). However, hydrate induction time will be prolonged at high sand concentration, because several researchers have found the thermodynamic inhibition effect of sand for hydrate formation (Aladko et al., 2004; Kang and Lee, 2010; Pan et al., 2018; Prasad et al., 2012; Saw et al., 2015; Wang et al., 2019a; Wen et al., 2019; Yang et al., 2012; Zhang et al., 2010). Moreover, for water in oil emulsion system with higher sand dosage, Pickering emulsion will form to hinder mass- and heat-transfer for hydrate nucleation. Sand particles sometimes will interact with the surfactants in the emulsion to affect hydrate formation (Ahuja et al., 2018). Meanwhile, Water film adsorbs on the outer surface of hydrophilic sand particles (Wang et al., 2019a). The inhibition heat and mass transfer effect can be reduced by particles collision to destroy the water film. The higher the sand concentration is, the more sand particle collision occurs. Therefore, the sand concentration in system has a great effect on hydrate formation. However, the influence mechanism of the presence and content of sand on the formation of hydrates is still unclear.

Furthermore, the size of sand particles also affects the formation of hydrates. Jiang et al. (2011) found that hydrate easily forms with a larger proportion in coarse sand. Sun et al. (2014) believed that hydrates are preferentially generated in large pore size with weak capillary force, because the stronger capillary force of small pores will reduce the activity of water, inhibit the diffusion of gas molecules, and hinder gas-liquid contact. However, Nair et al. (2016) pointed out that hydrate formation rate with small-sized sand is higher than that with large-sized sand, which caused by gas intake of the small-sized sand layer accelerating hydrate formation. The smaller the sand particle size is, the larger the specific-sufficient gas-liquid surface area is (Zhan et al., 2018; Zi et al., 2019). Thus, the hydrate growth rate increases with the decrease of gravel particle size (Nair et al., 2016; Zhang et al., 2020). Otherwise, Kang et al. (2009) found that the effect of pore size on hydrate formation rate could be ignored. Therefore, the influence of sand particle size on hydrate formation have not reached an unambiguous conclusion. Further study should be carried out.

After forming hydrates in a sandy multiphase fluid, the fluid transforms into a non-Newtonian fluid. Sand and hydrate particles will colly, bond and coalesce. This non-Newtonian fluid might have property of shear thinning, thixotropy and yield properties (Ahuja et al., 2015; Chen et al., 2019a; Rensing et al., 2011; Shi et al., 2017). During the NGHs exploitation and development, hydrates will decompose or form with the flow condition in this sandy multiphase fluid. It is difficult to determine its viscosity by merely using the published hydrate slurry viscosity prediction models during hydrate formation or decomposition process.

In this work, experiments are carried out to study the hydrate formation, dissociation, and viscosity in gas-water-sand system with sand concentrations of 0–5 wt% and sand particle size of 13–47 μm. The effects of sand particles on hydrate nucleation and growth are discussed. The viscosity characteristics of the sandy multiphase fluid during hydrate formation and dissociation are investigated. These findings fill in the knowledge blind spot of hydrate formation kinetics and hydrate slurry rheological behaviors with micron-sized sands in the flow system, which will be promoting high-efficiency and high-safety development of natural gas hydrates.

2. Experimental section

2.1. Materials

Materials used in the experiments include methane with a purity of 99.98% (Henan Xinshengyuan Chemical Co., Ltd.), quartz sand (Bright Quartz Sand Factory) and deionized water. In order to approach the actual scenario of natural gas hydrate development, quartz sand is used in this work to form a gas-water-sand system. Four kinds of micron-sized sands are selected, including 300 mesh, 400 mesh, 600 mesh and 1000 mesh, respectively. The Scanning Electron Microscope (SEM) figures of the quartz sand are shown in Fig. 1. According to Fig. 1, the surface of quartz sand is rough and irregular polyhedron. In the process of hydrate trial production in the South China Sea, the size of the sands in the wellbore is on the order of microns, while the micro morphology of natural sand is irregular. Therefore, the properties of quartz sand used in the experiments are close to those in the actual field engineering. The main component of quartz sand is silicon dioxide (SiO_2), with a density of 2.65 g/cm^3. And the sand used is insoluble in water. The relationships between the particle mesh and particle size are shown in Table 1.

2.2. Apparatus

The experimental apparatus is composed of a high-pressure gas cylinder, Anton-Paar rheometer MCR 101 with high-pressure (up to 15 MPa) section, and a data acquisition system. The outer radius and the inner radius of cylinder used in this work are 13.56 mm and 12.50 mm respectively, and the length of the cylinder is 37.5 mm. The schematic diagram is shown in Fig. 2. The temperature is achieved at the range of −20–150 °C by a chiller (DC-1006, Sunny Heng-Ping Scientific Instrument Company, Shanghai). The rheometer rotor used in the experiment is a blade impeller, which is shown in Fig. 3. More information of this apparatus can be found in our previous publications (Chen et al., 2019b; Shi et al., 2016, 2018).

2.3. Experimental procedures

The fixed experimental conditions are initial pressure of 8.8 MPa, cooling temperature of 274.15 K, water volume of 30 mL

Table 1
Relationship between the grain size and gravel mesh number.

No.	1	2	3	4
Mesh	300	400	600	1000
Maximum Particle Size, μm	47	38	23	13

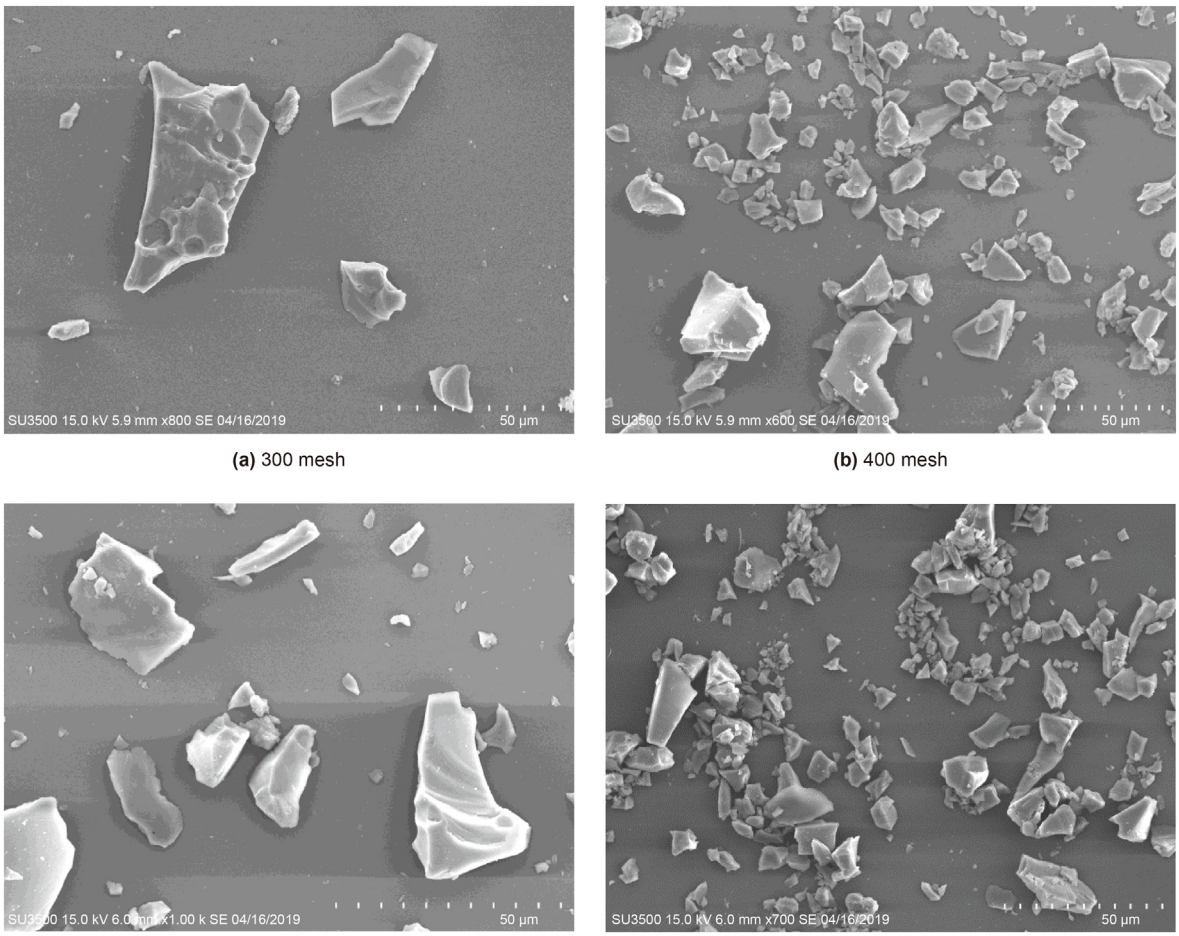

(a) 300 mesh **(b)** 400 mesh

(c) 600 mesh **(d)** 1000 mesh

Fig. 1. SEM images at four kinds of micron-sized quartz sand particles.

and shear rate of 700 s^{-1}. The other changed experimental conditions are shown in Table 2. Each experiment is repeated at least three times. The specific experimental procedure of case 2# is as follows.

1) Pressure the cylindrical cup of the rheometer up to 10 MPa for checking the tightness without a pressure change >0.05 MPa in a period of 5 h. Then remove gas waiting for liquid loading.
2) Measure 0.3 g quartz sand particle by using an electronic balance with an accuracy of 0.00001 g, and mix them into 30 mL deionized water with a fully stir until the sand particles evenly disperse in the liquid.
3) Inject the prepared liquid sample into the cylindrical cup of the rheometer.
4) Charge methane to 8.8 MPa through regulating valve V_1, V_2 and V_3 (Fig. 2) under the temperature of 20 °C for 40 min.
5) Start to shear test at 700 s^{-1} with a cooling rate of 0.5 °C/min to 1 °C.
6) The viscosity of sample increases and then remain stable after hydrate formation completes without a pressure change >0.05 MPa in a period of 30 min.
7) Set a heating rate of 0.2 °C/min to decompose hydrates.
8) After the pressure is restored and stabilized for 30 min, the experiment of case 2# is finished.
9) Relieve the pressure, remove the liquid sample and clean the apparatus.

3. Results and discussion

3.1. Hydrate formation in sandy multiphase fluid

The pressure and viscosity data during hydrate formation process in the sandy multiphase fluid is shown in Fig. 4. Three stages can be divided during hydrate formation (Heeschen et al., 2016; Shi et al., 2018), including gas dissolution, hydrate nucleation and growth.

In stage I, the viscosity data of the fluid is stable. There are two pressure drops in stage I. The first pressure drop is due to the small amount of gas dissolved in the liquid phase under the action of stirring. When the gas dissolved in the liquid phase is saturated, the pressure stabilizes and a plateau appears in the pressure curve. Subsequently, the temperature gradually decreases from the initial set temperature to the target temperature, which is realized by manual setting. As the temperature decreases, the solubility of the gas in the liquid phase increases, and the system pressure begins to decrease. When the gas dissolved in the liquid phase is saturated again, the pressure curve remains unchanged again.

In stage II, the pressure data changes slightly and the viscosity data of the fluid is still at the initial value. This period of stage II is the well-known induction time for hydrate nucleation. In stage III of hydrate growth, the pressure curve declines rapidly and the viscosity curve rises quickly. During the hydrate growth process, sand and hydrate particles will collide into aggregates basing on

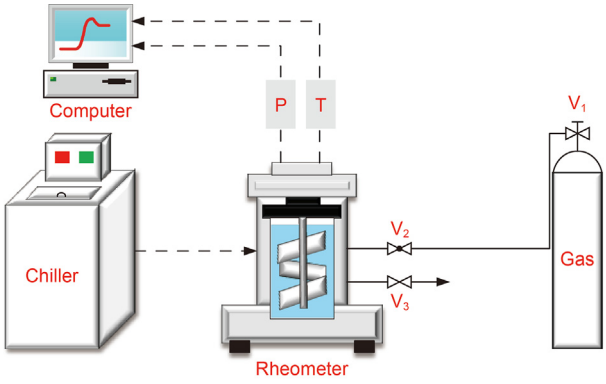

Fig. 2. Schematic diagram of fluid viscosity measurement system.

their hydrophilic surfaces with strong liquid bridging adhesion (Shi et al., 2017). Due to the mass- and heat-transfer limitation, pressure curve tends to be flat and the hydrate formation is completed in the end of Fig. 4.

3.1.1. *Effects of sand concentration and particle size on induction time*

The induction time for this work is defined as the time period of stage II (Fig. 4). Detailed data of the induction time are listed in Table 3. For pure water system, the induction time is 0.8533 h. To discuss the effects of sand concentration and particle size on induction time, a new dimensionless parameter of induction time, η_t, is defined as the hydrate induction time ratio of sandy and pure water system. Only for Cases 4# and 12#, it is below 1.0 with the sand particle size of 600 mesh. For the other experiments with sands, the induction time is prolonged, indicating that hydrate nucleation is inhibited. Furthermore, it should be noted that the hydrate nucleation is quite random. The induction times of repeated experiments for the same conditions varies widely. The uncertainty in Table 3 can indicate this phenomenon. Overall, the effect of the sands on the induction time is relatively small.

The mean value of repeated experiments is used for analysing the experimental data. According to the information shown in Fig. 5a, the inhibition effect of sand particles on hydrate nucleation decreases with the increase of sand concentration at the particle size of 1000 mesh. Among all the sandy experiments, the longest induction time is 1.942 h with a sand concentration of 1 wt% of at 1000 mesh (Case 5#), which is at just the smallest sand particle size and the lowest sand concentration. For the results of induction time at larger particle sizes of 300–600 mesh with sand concentration of 1 wt%~5 wt%, the maximum inhibition effect is observed at a middle sand concentration of 3 wt% as shown in Fig. 5b. Compared with other cases with the same sand concentration, cases No.4#, 8#, and 12# have a smallest η_t. 600 mesh is probably a critical size.

Water is bound to the hydrophilic surface of the sand particles by forming hydrogen bonds with the hydroxyl groups, making water difficult to form hydrate cage structures (Wang et al., 2017). Meanwhile, the capillarity in the hydrate-fine-sand to form the

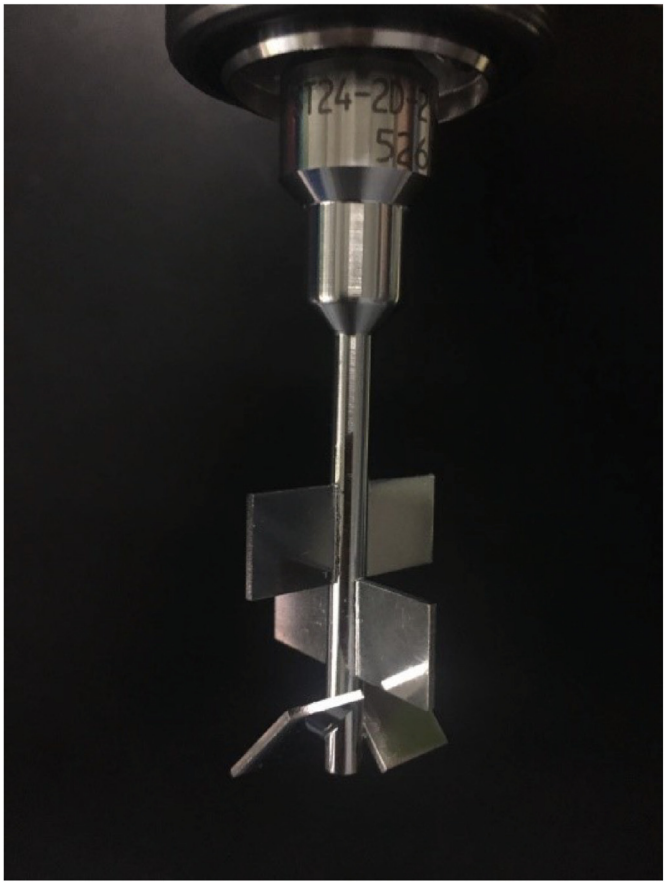

Fig. 3. The stirring paddle used in this work.

Table 2
Experimental conditions.

Case No.	Sand concentration, wt%	Sand particle size (mesh)
1#	0	Not applicable
2#	1	300
3#		400
4#		600
5#		1000
6#	3	300
7#		400
8#		600
9#		1000
10#	5	300
11#		400
12#		600
13#		1000

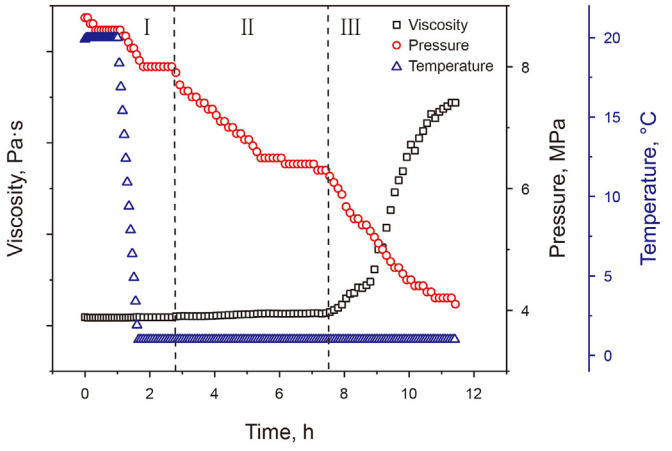

Fig. 4. Pressure, temperature, and viscosity data during methane hydrate formation process in sandy multiphase fluid (Case 2#).

Table 3
Results of induction time for sandy system.

No.	Induction Time, h	Uncertainty, h	η_t	No.	Induction Time, h	Uncertainty, h	η_t
2#	1.197	0.45	1.402	8#	1.077	0.56	1.262
3#	1.725	0.38	2.021	9#	1.540	0.30	1.805
4#	0.677	0.16	0.793	10#	1.160	0.29	1.359
5#	1.942	0.47	2.276	11#	1.493	0.20	1.749
6#	1.792	0.73	2.100	12#	0.800	0.071	0.938
7#	1.760	0.40	2.063	13#	1.172	0.049	1.373

additional surface tension will reduce the activity of water molecules (Pan et al., 2017; Sun et al., 2014; Wang et al., 2019b; Yang et al., 2012). The total solid-liquid interface area of fine sand particles is greater than that of large sand particles with the same sand concentration. Therefore, smaller particle size inhibits hydrate nucleation. On the other hand, the suspended sand particles in the bulk phase provide the interface for heterogeneous hydrate nucleation sites, thus shortening the induction time (Ahuja et al., 2018; Govindaraj et al., 2015; Heeschen et al., 2016; Linga et al., 2012; Nesterov et al., 2015; Pan et al., 2018; Prasad et al., 2012; Raman et al., 2016; Shi et al., 2018; Siangsai et al., 2015; Wang et al., 2017, 2019a; Zi et al., 2019). When the mass fraction of sand remains unchanged, the smaller the particle size, the more nucleation sites, which promote the nucleation of hydrates (Chari et al., 2013; Heeschen et al., 2016; Nesterov et al., 2015; Shi et al., 2017, 2018; Siangsai et al., 2015; Wang et al., 2019a; Zi et al., 2019). In conclusion, the concentration and particle size of sand particles have both promotion and inhibition effects on the induction time of hydrate formation (Pan et al., 2017; Said et al., 2016).

In summary, the experimental data of this work reflect that sands have a low inhibitory effect on hydrate nucleation. However, it should be recognized that due to the strong randomness of hydrate nucleation, the research in this work is far from enough, and more repeated experiments should be performed to investigate the hydrate nucleation from a probabilistic perspective.

3.1.2. Effects of sand concentration and particle size on hydrate growth

Results of total hydrate volume fraction under various sandy experimental conditions are listed in Table 4. For pure water system, the total hydrate volume fraction is 0.1723. To discuss the effects of sand concentration and particle size on hydrate formation volume, a dimensionless parameter of hydrate volume fraction, η_v, is defined as the hydrate formation volume ratio of sandy and pure water system. These relative hydrate volume fractions are shown in Fig. 6. According to our experimental results, the difference of hydrate formation amount in various cases is not obvious. The concentration and particle size of sand in this work have little effect on the kinetics of hydrate formation.

From the data shown in Fig. 6a, total hydrate formation volume fractions under all the experiments with the sand concentration of 1 wt%, are greater than that in sandy system. For the results at the sand concentration of 3 wt% and 5 wt%, the values of η_v are greater than 1.0 at sand particle size of 400 mesh and 1000 mesh; the values of η_v are below 1.0 at sand particle size of 300 mesh and 600 mesh. From the data shown in Fig. 6b, total hydrate formation volume fractions under all the experiments with the sand particle size of 400 mesh and 1000 mesh, are greater than that in other sandy system. For the results at the sand particles size of 300 mesh and 600 mesh, the values of η_v are greater than 1.0 at lower sand concentration 1 wt% and the values of η_v are below 1.0 at a higher sand concentration of 3 wt% or 5 wt%. The maximum total hydrate volume fraction is 0.1944 in Case 3#, and the minimum total hydrate volume fraction is 0.1682 in Case 12#. However, the overall changes are not significant, which is similar to Wang et al.'s conclusion (Wang et al., 2017).

The significant contributions to enhance the hydrate formation amount can be seen at an intermediate particle size of 400 mesh (Fig. 6a), and they also can be found with the smallest sand concentration of 1 wt% (Fig. 6b). Under a constant sand concentration, the hydrate formed under the condition of 400 mesh is the largest, which may be a critical sand particle size. The similar conclusion has been reported by Heeschen et al. (2016).

Different from the mechanism of hydrate nucleation, mass- and heat-transfer resistance is the key to hydrate growth (Shi et al., 2022). When the particle size is small, the liquid-solid interface area is large, resulting in more bound liquid water on the particle surface, and the liquid water will be trapped in the hydrates-sands aggregate during the hydrate growth process. Due to the influence of mass transfer resistance, it is difficult for the bound liquid water to be converted into hydrates, resulting in lower hydrate formation amount. On the other hand, the smaller the particles, the easier it is to suspend in the liquid phase, and the greater the frequency of collision between particles. The mass transfer resistance can be reduced to a certain extent, thereby promoting hydrate formation amount. In a word, both promoting and inhibiting effects on hydrate formation have been found in the sandy multiphase fluid.

3.2. Viscosity of sandy multiphase fluid during hydrate formation

3.2.1. Viscosity of hydrate slurry

Fig. 7 shows the variation of viscosity characteristics during methane gas hydrate formation. There are three variation modes of viscosity curve of hydrate slurry in hydrate-sand system, namely S type, Steep drop type and Fluctuation type. As for the cause of this phenomenon, to be honest, there is no definite conclusion yet, and we are continuing to conduct continuous research. It is worth noting that these three types of changes are ubiquitous in the sand-hydrate suspension system.

The black curve in Fig. 7 shows a steep-dropping variation pattern. In a short period of time, the hydrates formation leads to a sharp increase in viscosity and a decrease in viscosity in the following short period of time. The viscosity curve has a steep period and is eventually stabilized. As shown in Fig. 8, hydrates are initially formed at the gas-liquid interface, including the interface between the upper gas phase and the lower liquid phase in the reactor, and the surface of bubbles in the liquid phase. The hydrate layer at the gas-liquid interface gradually thickens with the hydrate formation. Whereas, the shear action of the external stirring paddle can shatter the thin hydrate layer, causing the slurry viscosity to drop. Eventually, the microstructure in the slurry is arranged in order and the viscosity tends to be stable (Shi et al., 2017; Webb et al., 2014; Zi et al., 2019). In addition, the thixotropy of slurry also causes the decrease of viscosity because of the constant shear rate during the experiment (Ahuja et al., 2015; Karanjkar et al., 2016).

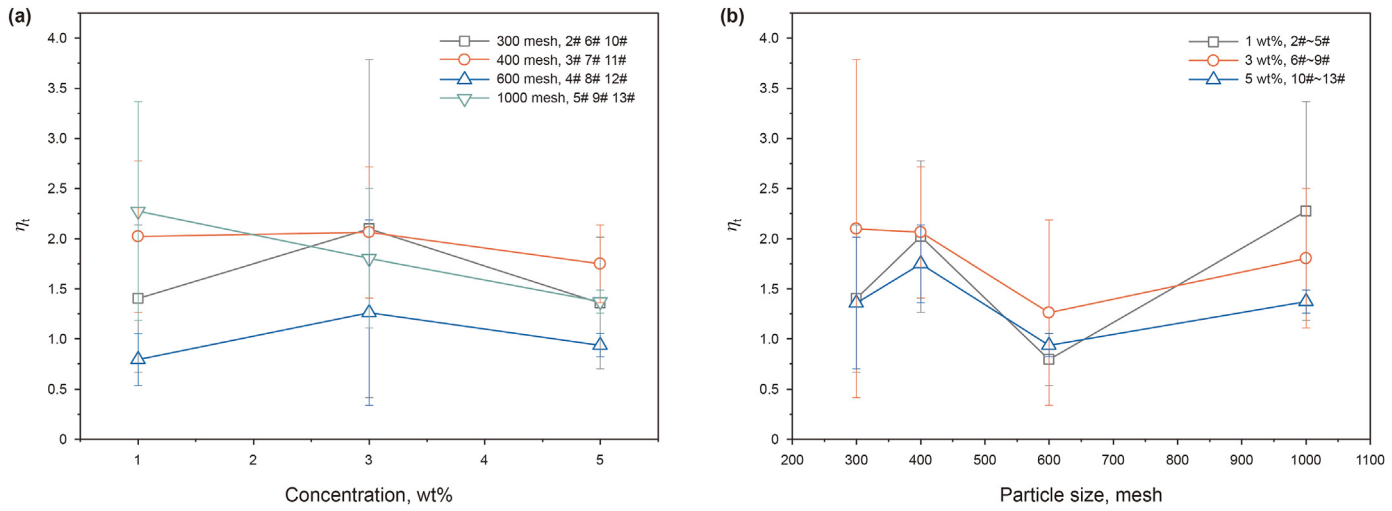

Fig. 5. Results of induction time dimensionless parameter η_t (a: trends of data with various sand concentrations; b: trends of data with various particle sizes).

Table 4
Results of the total hydrate volume fraction in sandy system.

No.	Total hydrate volume fraction	Uncertainty	η_v	No.	Total hydrate volume fraction	Uncertainty	η_v
2#	0.184	0.0092	1.065	8#	0.170	0.0072	0.987
3#	0.194	0.0071	1.128	9#	0.175	0.0063	1.015
4#	0.186	0.0083	1.081	10#	0.172	0.014	0.999
5#	0.178	0.0028	1.035	11#	0.190	0.0051	1.105
6#	0.170	0.0051	0.986	12#	0.168	0.0076	0.977
7#	0.181	0.011	1.053	13#	0.182	0.012	1.054

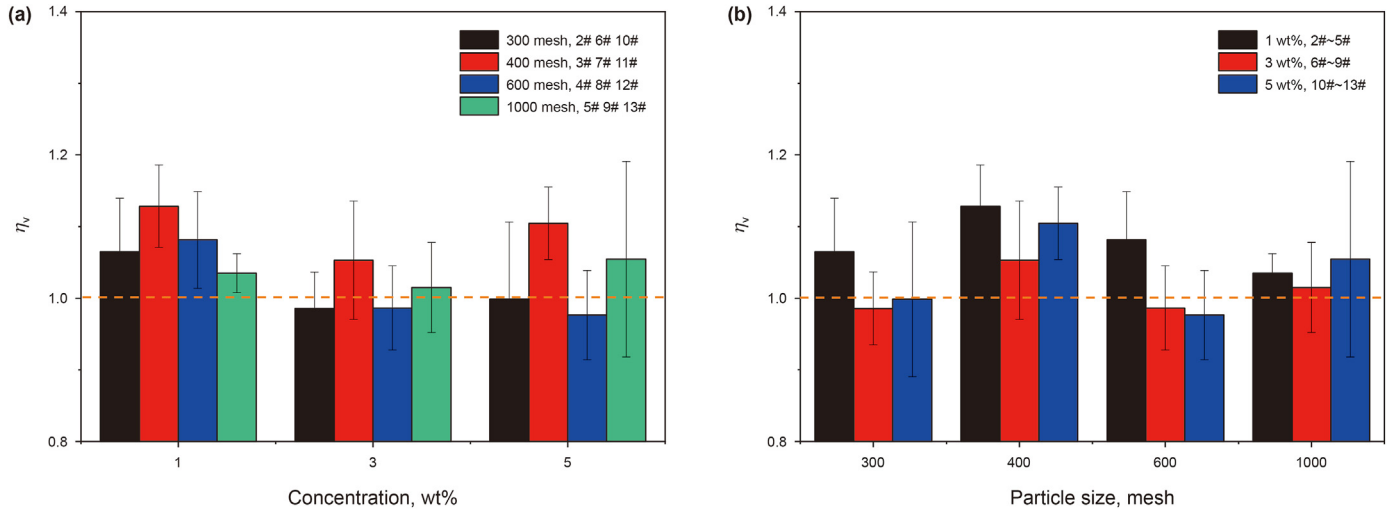

Fig. 6. Results of hydrate volume fraction dimensionless parameter η_v (**a**: trends of data with various sand concentrations; **b**: trends of data with various particle sizes).

The red curve in Fig. 7 shows the S-type variation pattern. Before the viscosity reaches the maximum, it is consistent with the characteristics of the Steep drop type curve. After reaching the highest value, the viscosity curve gradually tends to be stable, and the overall curve is S-shaped. The possible reason may be that a hydrate layer does not appear during the hydrate formation, and the hydrate particles are uniformly distributed in the liquid phase to form a stable sand-hydrate suspension. Therefore, the viscosity gradually increases and eventually tends to be stable, thus the viscosity curve is S-type.

The blue curve in Fig. 7 shows a fluctuation variation pattern. Whether the viscosity of the suspension during hydrate formation is stable is the key to distinguish the Fluctuation type from the other two types. The viscosity curve will fluctuate violently in a period of time. During hydrate formation, the dissolved gas is consumed during hydrate formation and then hydrate particles are formed. As shown in Fig. 8, hydrate particles aggregate due to continuous collisions to form hydrate aggregates. A hydrate layer may also form at the gas-liquid interface. These phenomena lead to

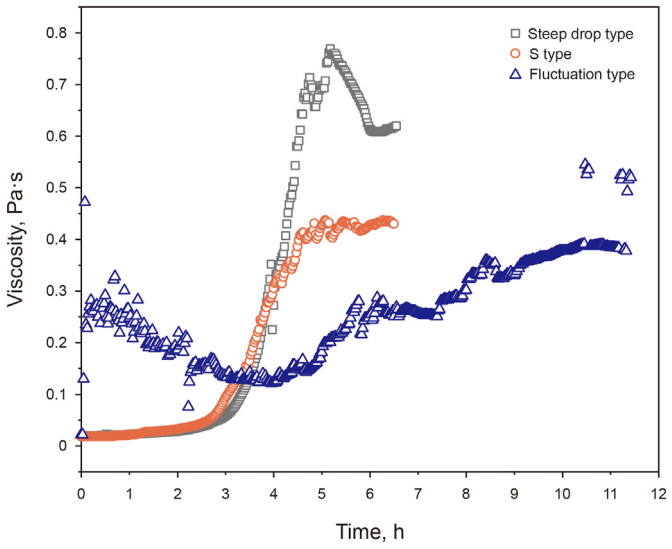

Fig. 7. Curve of viscosity characteristics of hydrate slurry in the formation process.

an increase in slurry viscosity. However, due to the shear action of the stirring paddle, the hydrate aggregates and hydrate layer are destroyed and the enclosed liquid is released, which leads to the decrease of slurry viscosity. Due to the randomness of hydrate formation process and the presence of stirring action, the colliding-destroying process is repeated during hydrate formation, so the viscosity curve will fluctuate violently. For the slurry system with high hydrate conversion rate, the blocking and sliding of some sand particles that never participated in the formation process and large size hydrate aggregates may also lead to the appearance of fluctuation curve (Liu et al., 2020).

In fact, the three variation modes of hydrate slurry viscosity appear randomly under various sand concentrations and particle sizes. Even if repeated under the same experimental conditions, all three variation modes are likely to evenly appear. In addition, some curves may have the characteristics of multiple modes during one experiment. For example, the viscosity change is S-type in the early stage, followed by violent fluctuations.

3.2.2. Maximum viscosity of hydrate slurry

As described in 3.2.1, due to the various change modes of the viscosity curve during the experiment, it is difficult to qualitatively describe the influence of sand particles on the change of slurry viscosity during hydrate formation. In this section, μ_{max} is applied to characterize the maximum viscosity of slurry during the hydrate formation process in the hydrate-sand system, and the average values of the results of several experiments are provided. The experimental results are shown in Table 5 and Fig. 9. Results show that the variations of viscosity and hydrate formation volume fraction are basically consistent in No.2, 3, 5–7, 9–11 and, 13 experiments. The reason is that the viscosity of slurry is determined by sand particles and hydrate aggregates in the system. On one hand, the solid sand particles are floating in the liquid phase, increasing the slurry viscosity. On the other hand, the existence of liquid bridging force between hydrate particles leads to the continuous aggregation of particles and the formation of larger hydrate particles, which increases the viscosity of the slurry. Therefore, the maximum value of viscosity corresponds to the volume fraction of hydrate. Among them, the 300-mesh sand particle size is relatively large, so the maximum value of viscosity will be significantly increased at the concentration of 5 wt% compared with 3 wt%, showing the phenomenon of low hydrate volume fraction but high viscosity peak, but there is little difference between the two values. Besides, in experiment No.4, the hydrate volume fraction is less than that at the concentration of 3 wt% or

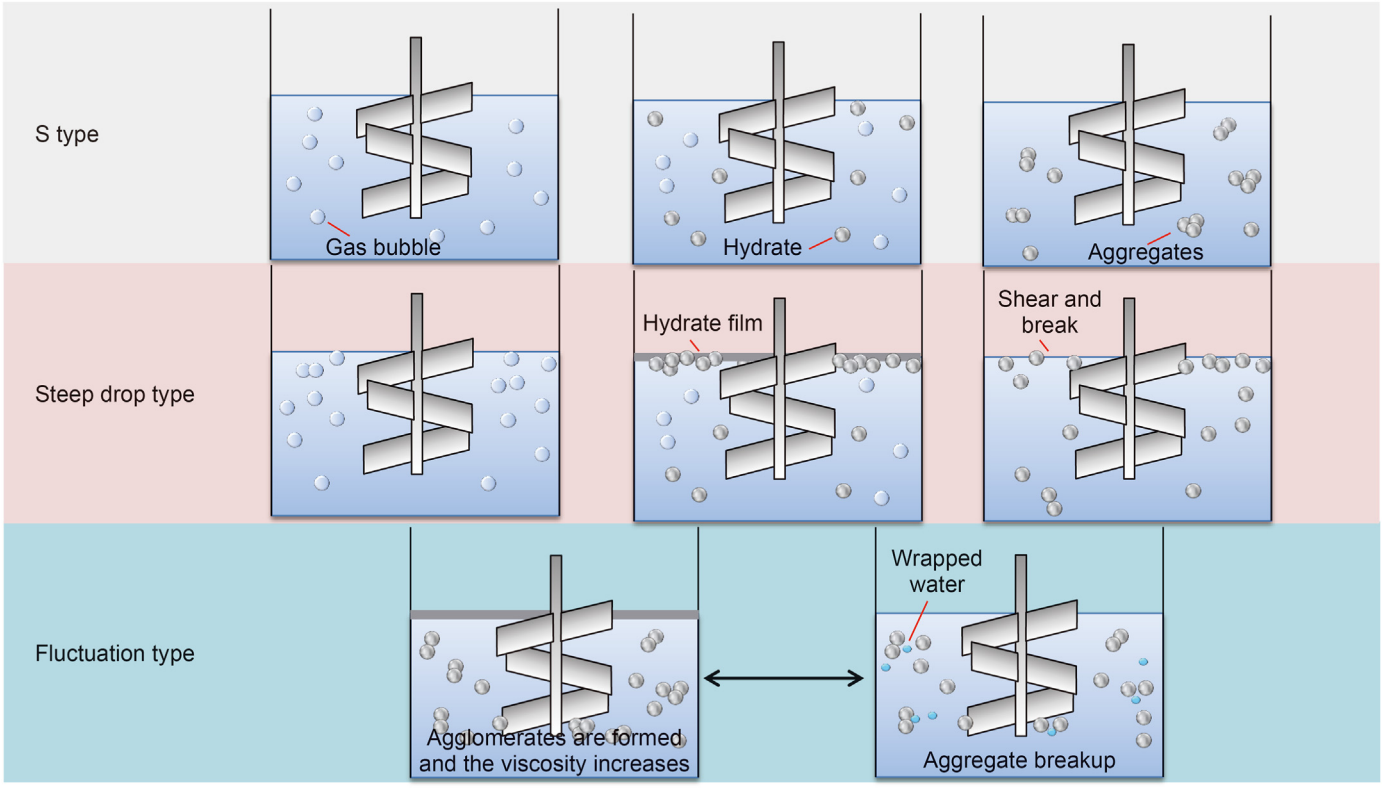

Fig. 8. Schematic diagram of viscosity variation mode during hydrate formation.

Table 5
Viscosity maximum of hydrate slurry during formation process.

No.	μ_{max} Pa·s	Uncertainty	No.	μ_{max} Pa·s	Uncertainty	No.	μ_{max} Pa·s	Uncertainty
2#	1.004	0.519	6#	0.514	0.114	10#	0.623	0.390
3#	0.578	0.131	7#	0.681	0.224	11#	0.665	0.136
4#	0.772	0.105	8#	0.793	0.257	12#	0.497	0.178
5#	1.177	0.497	9#	0.536	0.206	13#	0.565	0.130

5 wt%. Most of the hydrate particles are formed at the gas-liquid interface and then form a thin layer, and the lower sand concentration causes most of the sand particles to be wrapped in the center of hydrate particles, resulting in a large shear resistance of hydrate thin layer breaking at the interface, therefore, the measured slurry viscosity peak is high. With the increase of sand concentration, the collision of sand particles is enhanced, and the hydrate particles disperse more evenly in the slurry, resulting in the decrease of peak viscosity.

3.3. Hydrate dissociation in sandy multiphase fluid

3.3.1. Viscosity of hydrate slurry

Taking No.2 experiment as an example, Fig. 10 shows the viscosity and pressure changes of hydrate slurry in the process of heating dissociation. It shows that the hydrate dissociation process is also divided into three stages.

Stage I: Self-preservation process during hydrate dissociation. With the gradual increase in temperature, a small amount of hydrate particles decomposes. However, there is a self-preservation effect in the dissociation (Chen et al., 2021), and the surface of hydrate particles will freeze and hinder the further dissociation of hydrates (Zhou et al., 2016). In addition, a small amount of methane molecules generating from the dissociation will contact with water again, which may lead to the secondary hydrate growth (Wen et al., 2019; Zhou et al., 2016), so the viscosity increases slightly. In fact, this stage continues, but the rise of viscosity is not observed in all experiments due to the randomness of shear crushing and the influence of temperature. At this stage, a small amount of gas escapes due to the rise of temperature, and the pressure increases slightly or remains almost unchanged.

Stage II: Large scale dissociation process of hydrate. The continuous rise of temperature gradually weakens the self-protection effect, a large number of hydrate particles decompose in a short time and the viscosity decreases rapidly. In addition, a significant pressure increase is observed due to the release of large amounts of gas.

Stage III: Stable dissociation process. At this stage, the hydrates basically decompose completely, and the viscosity remains almost unchanged. Due to the relatively high temperature, the dissolved gas is precipitated, and the pressure shows a small upward trend, but it is still basically stable.

3.3.2. Comparison of viscosity characteristics

Fig. 11 illustrates the relationship between the viscosity and the hydrate volume fraction during hydrate formation and decomposition. During the formation process, the viscosity of the slurry increases with the increase of the hydrate volume fraction. Even with the same hydrate volume fraction, the viscosity of the slurry during the formation process is higher than that during the dissociation process. In dissociation process, the viscosity changes little at different hydrate volume fractions, which may be ascribed to the fact that the temperature rise causes the viscosity of the continuous phase to decrease during the dissociation process. In addition, the rise in temperature will weaken the liquid bridging force between the hydrate particles and disperse the aggregates. Finally, the continuous phase in the gap is released. Therefore, when the hydrate volume fractions in the system are the same in the formation process and dissociation process, the viscosity of the slurry in formation process is significantly higher than that in dissociation process, which needs further research.

Fig. 12 shows the curves of the hydrate volume fraction versus time during formation and dissociation process in 300 mesh and 400 mesh gas-water-hydrate-sand systems at various concentrations. The change of the hydrate volume fraction in dissociation process is significantly faster than that in the formation stage, and the change curves of the dissociation process at different

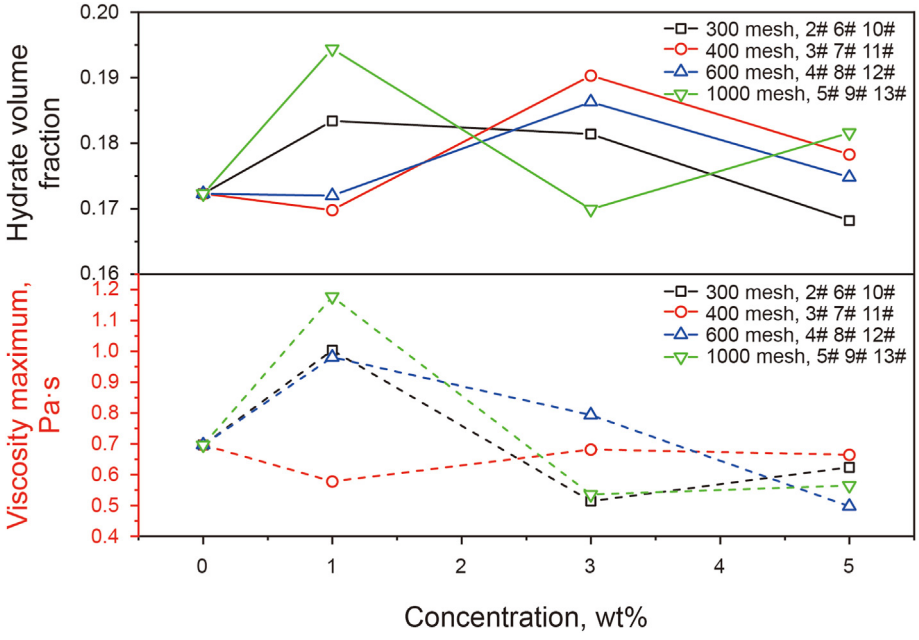

Fig. 9. Relationship between hydrate volume fraction and the maximum value of viscosity.

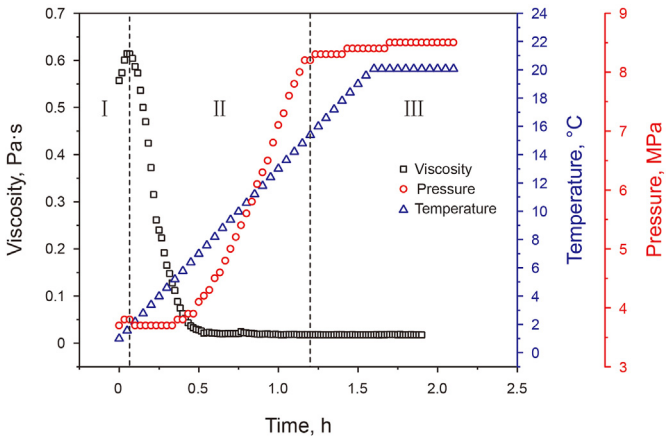

Fig. 10. Changes of viscosity, pressure, and temperature during dissociation (300 mesh, 1 wt%).

concentrations are similar. The difference is only obvious in the formation process. In the actual process of NGHs development using the solid fluidization mining method, it cannot directly correspond to the characteristics of the slurry in dissociation process when the characteristics of the hydrate slurry in formation process are known. It is worth noting that the driving mode of depressurization and heating has a critical influence on the dissociation kinetics of hydrates, and the viscosity behaviors during decompression and other dissociation processes are still unclear. Therefore, the rheological properties of hydrate slurry during hydrate dissociation need to be further studied.

4. Conclusion

In this paper, a high-pressure rheometer equipped with a stirring paddle is applied to study the effects of micro-sized sands on methane hydrates formation, dissociation, and viscosity in gas-water-sand system. The conclusions are as follows.

(1) The hydrate induction time in the sandy system is slightly prolonged compared to the pure gas-water system. When the sand concentration changes in the range of 1–5 wt%, its inhibition effect first strengthens and then weakens with the increase in sand concentration. The induction time with 600 mesh is short, and it may even be lower than that in pure gas-water system at 1 wt% or 5 wt%. When the sand concentration is constant, the induction time shows a trend of shortening-prolonging with the decrease of sand particle size. It should be recognized that due to the strong randomness of hydrate nucleation, the research in this work is far from enough, and more repeated experiments should be performed to investigate the hydrate nucleation from a probabilistic perspective.

(2) The difference of hydrate formation amount in various cases is not obvious. The concentration and particle size of sand in this work have little effect on the kinetics of hydrate

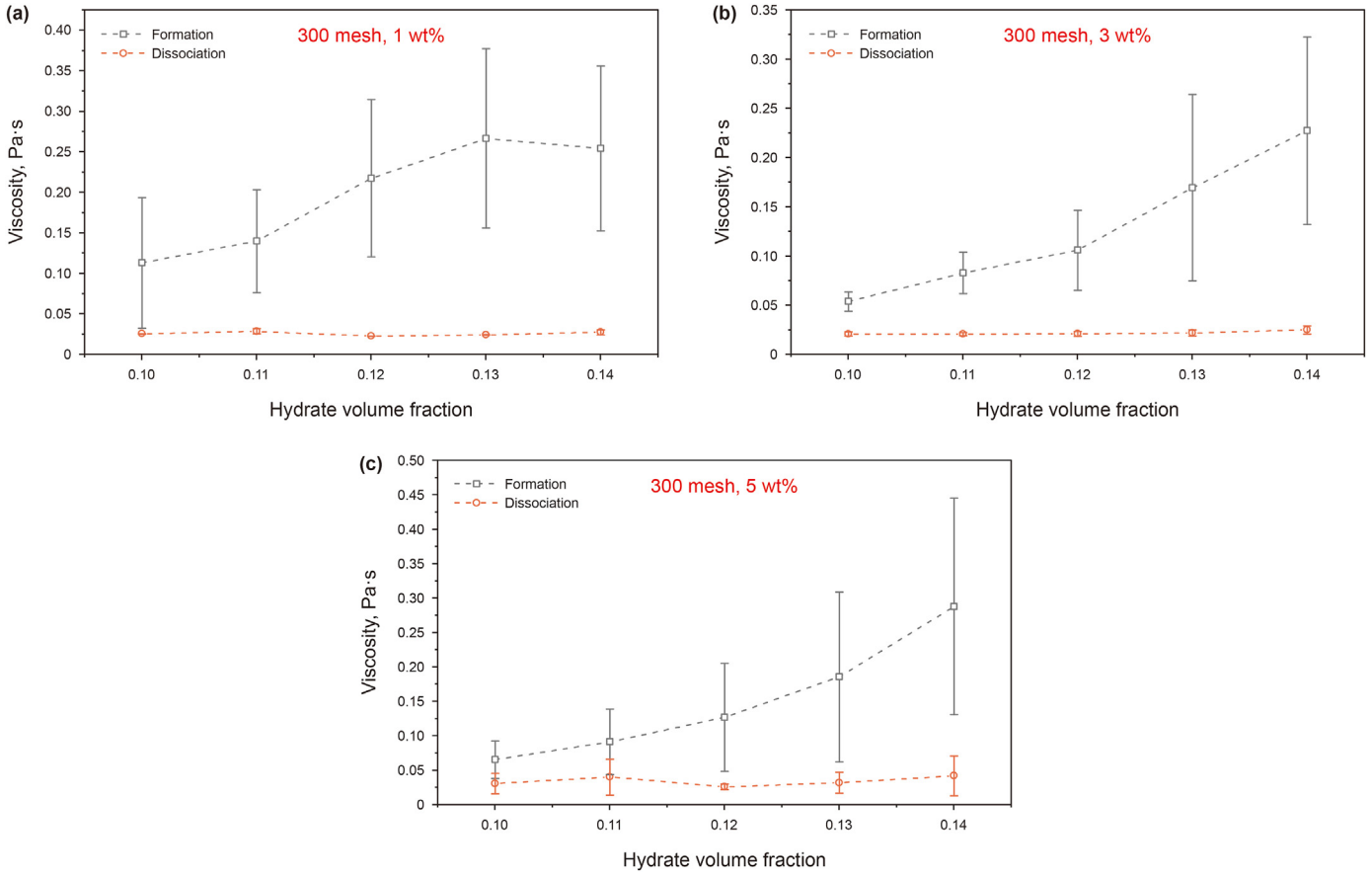

Fig. 11. The comparison of viscosity under the same hydrate volume fraction (300 mesh).

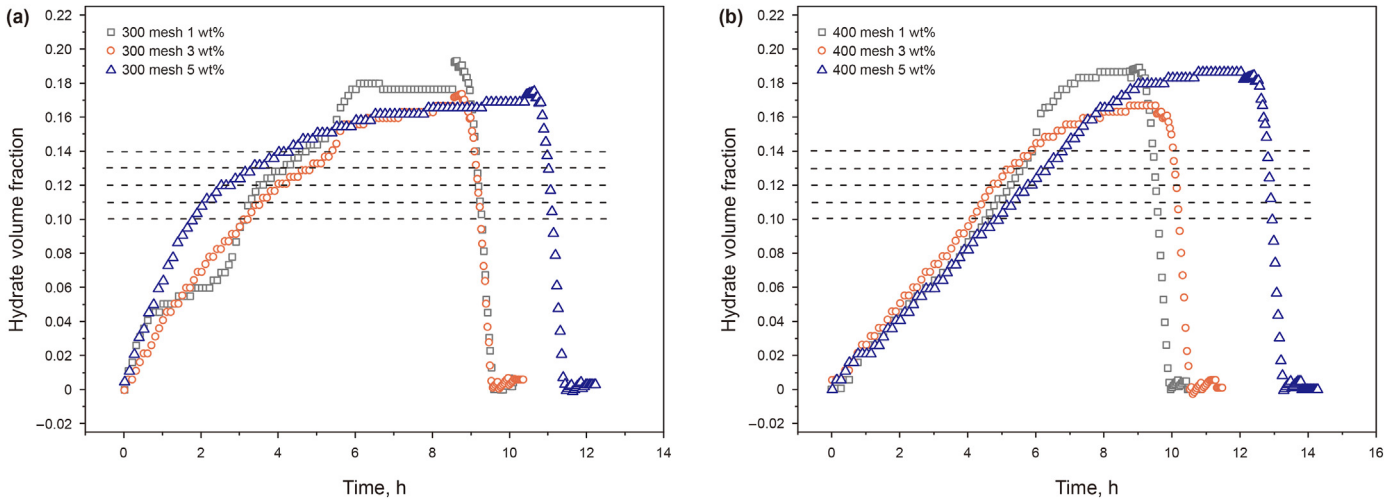

Fig. 12. Curves of hydrate volume fraction with time in the process of formation and dissociation ((**a**)300 mesh (**b**)400 mesh).

formation. Both promoting and inhibiting effects on hydrate formation have been found in the sandy multiphase fluid.

(3) In the process of hydrate formation, there are three modes of viscosity change: steep-dropping type, S-type and Fluctuating type. The three variation modes of hydrate slurry viscosity appear randomly under various sand concentrations and particle sizes.

(4) The viscosity of the slurry in formation process is significantly higher than that in dissociation process even if the hydrate volume fractions are the same, which means that the characteristics of the slurry in the hydrate formation process and the dissociation process need to be studied separately.

Acknowledgments

This work is supported by the National Natural Science Foundation of China [Grand numbers: 52104069, 51874323, U20B6005]; China Postdoctoral Science Foundation [Grand number: 2022M713460]; Science Foundation of China University of Petroleum, Beijing [Grand number: 2462020YXZZ045], all of which are gratefully acknowledged. Thanks to 4 anonymous reviewers for their contributions to improve the quality of this work.

References

Ahuja, A., Iqbal, A., Iqbal, M., Lee, J.W., Morris, J.F., 2018. Rheology of hydrate-forming emulsions stabilized by surfactant and hydrophobic silica nanoparticles. Energy Fuels 32 (5), 5877–5884. https://doi.org/10.1021/acs.energyfuels.8b00795.

Ahuja, A., Zylyftari, G., Morris, J.F., 2015. Yield stress measurements of cyclopentane hydrate slurry. J. Non-Newtonian Fluid Mech. 220, 116–125. https://doi.org/10.1016/j.jnnfm.2014.11.007.

Aladko, E.Y., Dyadin, Y.A., Fenclonov, V.B., Larionov, E.G., Mel'gunov, M.S., Manakov, A.Y., Nesterov, A.N., Zhurko, F.V., 2004. Dissociation conditions of methane hydrate in mesoporous silica gels in wide ranges of pressure and water content. J. Phys. Chem. B 108 (42), 16540–16547. https://doi.org/10.1021/jp048389q.

Chari, V.D., Sharma, D.V.S.G.K., Prasad, P.S.R., Murthy, S.R., 2013. Methane hydrates formation and dissociation in nano silica suspension. J. Nat. Gas Sci. Eng. 11, 7–11. https://doi.org/10.1016/j.jngse.2012.11.004.

Chen, J., Zeng, Y.S., Yu, X.Y., Yuan, Q., Wang, T., Deng, B., Yan, K.L., Jiang, J.H., Tao, L.M., Chen, C.Z., 2021. A covering liquid method to intensify self-preservation effect for safety of methane hydrate storage and transportation. Petrol. Sci. https://doi.org/10.1016/j.petsci.2021.11.007.

Chen, Y., Shi, B., Li, W., Huang, F., Lu, X., Liu, Y., Wu, H., Gong, J., 2019a. Progress of the non-Newtonian properties of hydrate slurry and viscosity model. Chem. Ind. Eng. Prog. 38 (6), 2682–2696. https://doi.org/10.16085/j.issn.1000-6613.2018-1817.

Chen, Y., Shi, B., Liu, Y., Ma, Q., Song, S., Ding, L., Lv, X., Wu, H., Wang, W., Yao, H., Gong, J., 2019b. In situ viscosity measurements of a cyclopentane hydrate slurry in waxy water-in-oil emulsions. Energy Fuels 33 (4), 2915–2925. https://doi.org/10.1021/acs.energyfuels.8b04268.

Englezos, P., 1993. Clathrate hydrates. Ind. Eng. Chem. Res. 32 (7), 1251–1274. https://doi.org/10.1021/ie00019a001.

Englezos, P., 2019. Extraction of methane hydrate energy by carbon dioxide injection-key challenges and a paradigm shift. Chin. J. Chem. Eng. 27 (9), 2044–2048. https://doi.org/10.1016/j.cjche.2019.02.031.

Govindaraj, V., Mech, D., Pandey, G., Nagarajan, R., Sangwai, J.S., 2015. Kinetics of methane hydrate formation in the presence of activated carbon and nano-silica suspensions in pure water. J. Nat. Gas Sci. Eng. 26, 810–818. https://doi.org/10.1016/j.jngse.2015.07.011.

Heeschen, K.U., Schicks, J.M., Oeltzschner, G., 2016. The promoting effect of natural sand on methane hydrate formation: grain sizes and mineral composition. Fuel 181, 139–147. https://doi.org/10.1016/j.fuel.2016.04.017.

Hong, B., Li, X., Song, S., Chen, S., Zhao, C., Gong, J., 2020. Optimal planning and modular infrastructure dynamic allocation for shale gas production. Appl. Energy 261, 114439. https://doi.org/10.1016/j.apenergy.2019.114439.

Jiang, G., Wu, Q., Zhan, J., 2011. The effects of cooling rate and particle size of medium to the formation of methane hydrate in sands. Nat. Gas Geosci. 22 (5), 920–925.

Jin, Y., Konno, Y., Nagao, J., 2012. Growth of methane clathrate hydrates in porous media. Energy Fuels 26 (4), 2242–2247. https://doi.org/10.1021/ef3001357.

Kang, S.P., Lee, J.W., 2010. Formation characteristics of synthesized natural gas hydrates in meso- and macroporous silica gels. J. Phys. Chem. B 114 (20), 6973–6978. https://doi.org/10.1021/jp100812p.

Kang, S.-P., Seo, Y., Jang, W., 2009. Kinetics of methane and carbon dioxide hydrate formation in silica gel pores. Energy Fuels 23 (7), 3711–3715. https://doi.org/10.1021/ef900256f.

Karanjkar, P.U., Ahuja, A., Zylyftari, G., Lee, J.W., Morris, J.F., 2016. Rheology of cyclopentane hydrate slurry in a model oil-continuous emulsion. Rheol. Acta 55 (3), 235–243. https://doi.org/10.1007/s00397-016-0911-1.

Liao, Q., Shi, B., Song, S., Duan, X., Yang, F., Gong, J., 2022. Molecular insights into methane hydrate growth in the presence of wax molecules. Fuel 324, 124743. https://doi.org/10.1016/j.fuel.2022.124743.

Linga, P., Daraboina, N., Ripmeester, J.A., Englezos, P., 2012. Enhanced rate of gas hydrate formation in a fixed bed column filled with sand compared to a stirred vessel. Chem. Eng. Sci. 68 (1), 617–623. https://doi.org/10.1016/j.ces.2011.10.030.

Liu, X., Hu, T., Pang, X., Xu, Z., Wang, T., Zhang, X., Wang, E., Wu, Z., 2021. Evaluation of natural gas hydrate resources in the South China Sea using a new genetic analogy method. Petrol. Sci. https://doi.org/10.1016/j.petsci.2021.12.004.

Liu, Z., Song, Y., Liu, W., Liu, R., Lang, C., Li, Y., 2020. Rheology of methane hydrate slurries formed from water-in-oil emulsion with different surfactants concentrations. Fuel 275. https://doi.org/10.1016/j.fuel.2020.117961.

Nair, V.C., Ramesh, S., Ramadass, G.A., Sangwai, J.S., 2016. Influence of thermal stimulation on the methane hydrate dissociation in porous media under confined reservoir. J. Petrol. Sci. Eng. 147, 547–559. https://doi.org/10.1016/j.petrol.2016.09.017.

Nesterov, A.N., Reshetnikov, A.M., Manakov, A.Y., Rodionova, T.V., Paukshtis, E.A., Asanov, I.P., Bardakhanov, S.P., Bulavchenko, A.I., 2015. Promotion and inhibition of gas hydrate formation by oxide powders. J. Mol. Liq. 204, 118–125. https://doi.org/10.1016/j.molliq.2015.01.037.

Pan, Z., Liu, Z., Liu, D., Shang, L., Li, W., Li, P., 2017. Research progress on influence factors of natural gas hydrate formation in porous media. Chem. Ind. Eng. Prog. 36 (12), 4403–4415 (in Chinese).

Pan, Z., Liu, Z., Zhang, Z., Shang, L., Ma, S., 2018. Effect of silica sand size and saturation on methane hydrate formation in the presence of SDS. J. Nat. Gas Sci. Eng. 56, 266–280. https://doi.org/10.1016/j.jngse.2018.06.018.

Prasad, P.S.R., Chari, V.D., Sharma, D.V.S.G.K., Murthy, S.R., 2012. Effect of silica particles on the stability of methane hydrates. Fluid Phase Equil. 318, 110–114. https://doi.org/10.1016/j.fluid.2012.01.012.

Raman, A.K.Y., Koteeswaran, S., Venkataramani, D., Clark, P., Bhagwat, S., Aichele, C.P., 2016. A comparison of the rheological behavior of hydrate forming emulsions stabilized using either solid particles or a surfactant. Fuel 179, 141–149. https://doi.org/10.1016/j.fuel.2016.03.049.

Rensing, P.J., Liberatore, M.W., Sum, A.K., Koh, C.A., Sloan, E.D., 2011. Viscosity and yield stresses of ice slurries formed in water-in-oil emulsions. J. Non-Newtonian Fluid Mech. 166 (14–15), 859–866. https://doi.org/10.1016/j.jnnfm.2011.05.003.

Said, S., Govindaraj, V., Herri, J.M., Ouabbas, Y., Khodja, M., Belloum, M., Sangwai, J.S., Nagarajan, R., 2016. A study on the influence of nanofluids on gas hydrate formation kinetics and their potential: application to the CO_2 capture process. J. Nat. Gas Sci. Eng. 32, 95–108. https://doi.org/10.1016/j.jngse.2016.04.003.

Saw, V.K., Udayabhanu, G., Mandal, A., Laik, S., 2015. Methane hydrate formation and dissociation in the presence of silica sand and bentonite clay. Oil & Gas Science and Technology-Revue D Ifp Energies Nouvelles 70 (6), 1087–1099. https://doi.org/10.2516/ogst/2013200.

Shi, B.-H., Chai, S., Ding, L., Chen, Y.C., Liu, Y., Song, S.F., Yao, H.Y., Wu, H.H., Wang, W., Gong, J., 2018. An investigation on gas hydrate formation and slurry viscosity in the presence of wax crystals. AIChE J. 64 (9), 3502–3518. https://doi.org/10.1002/aic.16192.

Shi, B.H., Chai, S., Wang, L.Y., Lv, X., Liu, H.S., Wu, H.H., Wang, W., Yu, D., Gong, J., 2016. Viscosity investigation of natural gas hydrate slurries with anti-agglomerants additives. Fuel 185, 323–338. https://doi.org/10.1016/j.fuel.2016.07.113.

Shi, B., Chai, S., Liu, Y., Ding, L., Song, S., Wu, H., Gong, J., 2017. Factors influencing the viscosity of natural gas hydrate slurry with wax crystal. Nat. Gas. Ind. 37 (5), 97–105. https://doi.org/10.3787/j.issn.1000-0976.2017.05.013.

Shi, B., Chen, Y., Wang, X., Song, S., Fu, S., Zhou, J., Liu, Y., Lv, X., Gong, J., 2022. Flowloop investigation into hydrate formation and slurry flow in the presence of micron-sized sand particles. J. Petrol. Sci. Eng. 212. https://doi.org/10.1016/j.petrol.2022.110251.

Shi, B., Song, S., Chen, Y., Duan, X., Liao, Q., Fu, S., Liu, L., Sui, J., Jia, J., Liu, H., Zhu, Y., Song, C., Lin, D., Wang, T., Wang, J., Yao, H., Gong, J., 2021. Status of natural gas hydrate flow assurance research in China: a review. Energy Fuels 35 (5), 3611–3658. https://doi.org/10.1021/acs.energyfuels.0c04209.

Siangsai, A., Rangsunvigit, P., Kitiyanan, B., Kulprathipanja, S., Linga, P., 2015. Investigation on the roles of activated carbon particle sizes on methane hydrate formation and dissociation. Chem. Eng. Sci. 126, 383–389. https://doi.org/10.1016/j.ces.2014.12.047.

Song, S., Shi, B., Yu, W., Ding, L., Chen, Y., Yu, Y., Ruan, C., Liu, Y., Wang, W., Gong, J., 2019. A new methane hydrate decomposition model considering intrinsic kinetics and mass transfer. Chem. Eng. J. 361, 1264–1284. https://doi.org/10.1016/j.cej.2018.12.143.

Sun, S.C., Liu, C.L., Ye, Y.G., Liu, Y.F., 2014. Phase behavior of methane hydrate in silica sand. J. Chem. Thermodyn. 69, 118–124. https://doi.org/10.1016/j.jct.2013.09.045.

Wang, R., Liu, T., Ning, F., Ou, W., Zhang, L., Wang, Z., Peng, L., Sun, J., Liu, Z., Li, T., Sun, H., Jiang, G., 2019a. Effect of hydrophilic silica nanoparticles on hydrate formation: insight from the experimental study. J. Energy Chem. 30, 90–100. https://doi.org/10.1016/j.jechem.2018.02.021.

Wang, W., Jiang, K., Li, Y., Shi, Z., Song, G., Duan, R., 2017. Kinetics of methane gas hydrate formation with microscale sand in an autoclave with windows. Fuel 209, 85–95. https://doi.org/10.1016/j.fuel.2017.07.063.

Wang, X.H., Wang, Y.F., Xie, Y., Sun, C.Y., Chen, G.J., 2019b. Study on the decomposition conditions of gas hydrate in quartz sand-brine mixture systems. J. Chem. Thermodyn. 131, 247–253. https://doi.org/10.1016/j.jct.2018.11.009.

Webb, E.B., Koh, C.A., Liberatore, M.W., 2014. High pressure rheology of hydrate slurries formed from water-in-mineral oil emulsions. Ind. Eng. Chem. Res. 53 (17), 6998–7007. https://doi.org/10.1021/ie5008954.

Wen, L., Zhou, X., Liang, D., 2019. Microscopic measurements on the decomposition behaviour of methane hydrates formed in natural sands. RSC Adv. 9 (26), 14727–14735. https://doi.org/10.1039/c9ra01611b.

Yang, M., Song, Y., Ruan, X., Liu, Y., Zhao, J., Li, Q., 2012. Characteristics of CO_2 hydrate formation and dissociation in glass beads and silica gel. Energies 5 (4), 925–937. https://doi.org/10.3390/en5040925.

Zhan, L., Wang, Y., Li, X.S., 2018. Experimental study on characteristics of methane hydrate formation and dissociation in porous medium with different particle sizes using depressurization. Fuel 230, 37–44. https://doi.org/10.1016/j.fuel.2018.05.008.

Zhang, L., Sun, M., Sun, L., Yu, T., Song, Y., Zhao, J., Yang, L., Dong, H., 2020. In-situ observation for natural gas hydrate in porous medium: water performance and formation characteristic. Magn. Reson. Imag. 65, 166–174. https://doi.org/10.1016/j.mri.2019.09.002.

Zhang, Y., Wu, H.J., Li, X.S., Chen, Z.Y., Li, G., Zeng, Z.Y., 2010. Dissociation behavior of methane hydrate in porous media. Chemical Journal of Chinese Universities-Chinese 31 (9), 1848–1854. https://doi.org/10.1109/ACP.2010.5682664.

Zhong, D.L., Lu, Y.Y., Sun, D.J., Zhao, W.L., Li, Z., 2015. Performance evaluation of methane separation from coal mine gas by gas hydrate formation in a stirred reactor and in a fixed bed of silica sand. Fuel 143, 586–594. https://doi.org/10.1016/j.fuel.2014.11.083.

Zhou, S., Chen, W., Li, Q., Zhou, J., Shi, H., 2017. Research on the solid fluidization well testing and production for shallow non-diagenetic natural gas hydrate in deep water area. China Offshore Oil Gas 29 (4), 1–8 (Chinese).

Zhou, X., Long, Z., Liang, S., He, Y., Yi, L., Li, D., Liang, D., 2016. In situ Raman analysis on the dissociation behavior of mixed CH_4-CO_2 hydrates. Energy Fuels 30 (2), 1279–1286. https://doi.org/10.1021/acs.energyfuels.5b02119.

Zhu, H.Y., Dang, Y.K., Wang, G.R., Zhou, S.W., Fu, Q., 2021. Near-wellbore fracture initiation and propagation induced by drilling fluid invasion during solid fluidization mining of submarine nature gas hydrate sediments. Petrol. Sci. 18 (6), 1739–1752. https://doi.org/10.1016/j.petsci.2021.09.026.

Zi, M., Chen, D., Wang, J., Hu, P., Wu, G., 2019. Kinetic and rheological study of methane hydrate formation in water-in-oil emulsion: effects of emulsion composition and silica sands. Fuel 255. https://doi.org/10.1016/j.fuel.2019.115708.